Journal of Magnetism and Magnetic Materials 518 (2021) 167367

Contents lists available at ScienceDirect

Journal of Magnetism and Magnetic Materials

journal homepage: www.elsevier.com/locate/jmmm

Research articles

# Spin-dependent Seebeck and Nernst effects in an ideal skyrmion gas

Andrei Zadorozhnyi, Yuri Dahnovsky*

*Department of Physics and Astronomy/3905, 1000 E. University Avenue, University of Wyoming, Laramie, WY 82071, United States*

ARTICLE INFO

*Keywords:*
Skyrmions
Topological spin Hall effect
Topological spin Seebeck and Nernst effects

ABSTRACT

We theoretically and numerically study spin-dependent Seebeck and Nernst effects in 2D ferromagnetic materials with the topological spin texture (skyrmion and vortex) ideal gas. From the numerical solution of the matrix Boltzmann equation for a nonequilibrium distribution function and the Lippmann–Schwinger equation for a T-matrix we find the strong nonlinear behaviors in the thermoelectric coefficients depending on skyrmion/vortex diameters and electron concentrations. In particular, the dramatic dependences in the Seebeck and Nernst coefficients take place at larger magnetic texture sizes where the abrupt sign flip in the vortex Seebeck and Nernst coefficients occurs in the narrow region of electron concentrations. In this case the normalized Nernst coefficient changes from + 5 to − 7. The spin-dependent thermoelectric coefficients are proportional to $T$ at low temperatures for all skyrmion/vortex sizes.

The Seebeck and Nernst effects take place when a voltage is induced by a temperature gradient between the two terminals of a device. If the device is a 2D (ferromagnetic) film with embedded magnetic moment textures, Seebeck and Nernst coefficients become spin-dependent. The Nernst coefficient can exist even in the absence of an applied magnetic field due to the presence of a constant magnetic moment. Much attention has been recently paid to the anomalous spin Seebeck and Nernst effects where the uniform magnetic moment causes the voltage difference along with and in the perpendicular direction to the applied temperature gradient. [1–8]

With the development of information technology, the energy harvesting is a key technology to control energy, through accumulation, storage, and use of power. Small-scale traditional natural energy sources such as heat, electromagnetic waves, etc. are known to be basic for energy harvesting devices. Thermoelectric energy sources can be useful to generate an electricity because of its clean heat conversion from ambient thermal sources. Especially it is a promising and challenging strategy to use magnetism in thermoelectric conversion. Thus, spin-dependent Seebeck (SDS) and Nernst (SDN) effects could be useful for future clean environmental technologies. [9,6,10].

Charge SDS and SDN effects take place when conduction electrons scatter at topological spin textures (skyrmions and vortexes). The presence of the *topological* spin textures differs SDS and SDN effects from the anomalous spin Seebeck and Nernst effects where the latter occur in a uniform ferromagnetic environment. To describe the topological spin thermoelectric effects we employ the following Hamiltonian:

$$H = \frac{k^2}{2m} - J\mathbf{S}(\mathbf{r})\cdot\boldsymbol{\sigma}, \tag{1}$$

where the first term represents the kinetic energy of conduction electrons, $J$ is an exchange integral, $\mathbf{S}(\mathbf{r})$ is a localized magnetic moment. Here $\boldsymbol{\sigma}$ is a vector with the three Pauli matrix projections for the conduction electron spins. We choose the $\mathbf{S}(\mathbf{r})$ texture in the following form:

$$\mathbf{S}(\mathbf{r}) = S_0\cdot\mathbf{e}_z + \sum_i \delta\mathbf{S}\left(\mathbf{r} - \mathbf{r_i}\right), \tag{2}$$

where $S_0$ is uniform out-of-plane background magnetization and $\delta\mathbf{S}(\mathbf{r} - \mathbf{r_i})$ is a deviation of magnetic moment due to the presence of the magnetic structure (in this work we only consider skyrmions with the topological charge $Q = 1$, and vortexes with the topological charge $Q = 0$). The main difference between the skyrmion with $Q = 1$ and vortex with $Q = 0$ is in a magnetic moment in the center of the texture. Indeed, for $Q = 1$ the magnetic moment equals the maximum value and for $Q = 0$ the magnetic moment is zero. The conduction electrons are a uniform electron gas embedded into the ferromagnetic/skyrmion environment. Because of the splitting of the energy for different spin projections, we can introduce two types of carriers depending on a spin orientation. For spin ↑ and spin ↓ we write the following energies $\varepsilon^{\uparrow,\downarrow}(\mathbf{k}) = \hbar^2k^2/(2m) \mp J$.

TSS, $\alpha$, and TSN, $Q$, coefficients are defined in the following way: [11]

* Corresponding author.
*E-mail address:* yurid@uwyo.edu (Y. Dahnovsky).

https://doi.org/10.1016/j.jmmm.2020.167367
Received 22 April 2020; Received in revised form 31 July 2020; Accepted 21 August 2020
Available online 17 September 2020

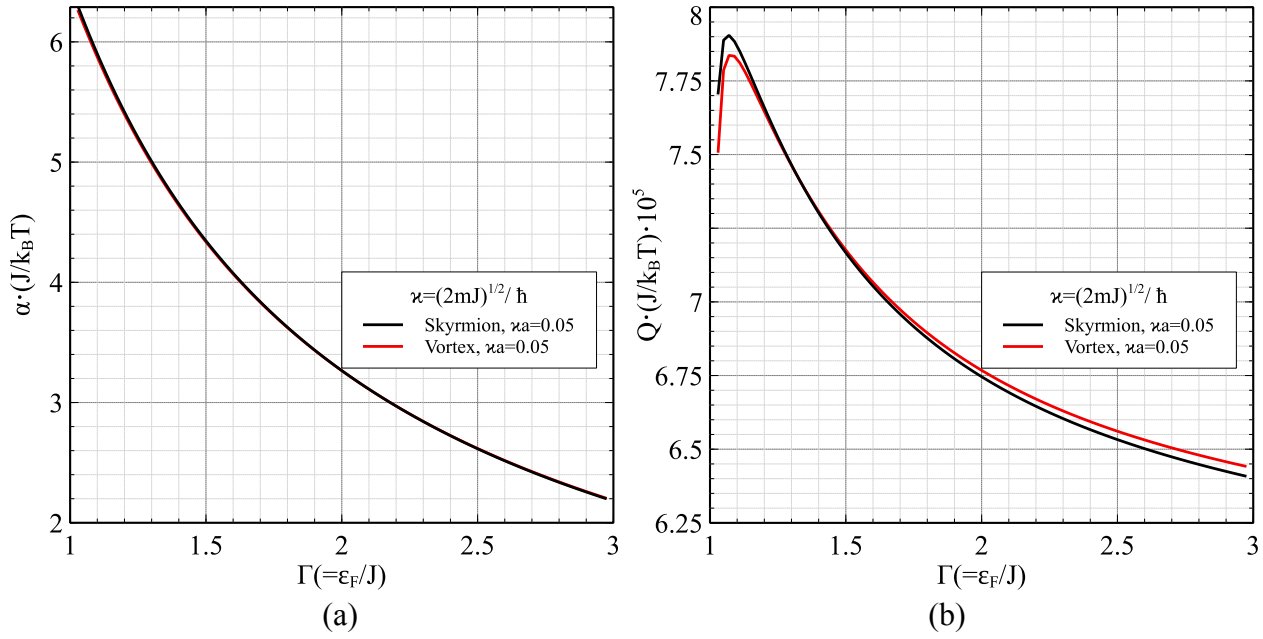


**Fig. 1.** (a) Seebeck coefficient and (b) Nernst coefficient for skyrmion/vortex sizes $\varkappa a = 0.05$.

$$\alpha = \frac{\nabla_x(e\varphi - \mu)}{\nabla_x(k_B T)}; \quad Q = \frac{\nabla_y(e\varphi - \mu)}{\nabla_x(k_B T)}, \tag{3}$$

where $\varphi$ is voltage, $\mu$ is chemical potential, and $T$ is a temperature.

To find $\alpha$ and $Q$, we solve the Boltzmann equation for a nonequilibrium distribution function, $f^s(\mathbf{k}) = f_0(\mathbf{k}) + f_1^s(\mathbf{k})$, $f_1^s(\mathbf{k}) = -(\partial f_0/\partial\varepsilon)\chi^s(\varepsilon)\cdot\mathbf{k}$, where $f_0$ is the Fermi equilibrium distribution function, $f_1$ is the nonequilibrium part, and $\chi^s$ is an unknown vector function depending on the electron energy. [11] The scattering mechanism is due to the interaction of the spins of the conduction electrons with the localized magnetic moment. Therefore, we consider an ideal gas of skyrmions. The stationary, time-independent Boltzmann equation appears to be $4 \times 4$ matrix equation,[12–14] which dimension is determined by x and y projections of $\chi^s$ and the two electron spin projections, ↑, ↓. The right-hand-side of the Boltzmann equation can be presented by the $2 \times 2$ transition probability per unit time matrix:

$$W_{\mathbf{pp}'}^{ss'} = \frac{2\pi}{\hbar} n_t \ |T_{\mathbf{pp}'}^{ss'}|^2 \delta\left(\varepsilon - \varepsilon'\right), \tag{4}$$

which due to the radial symmetry only depends on the angle between the incident and scattered directions. In Eq. (4) $n_t$ is a 2D density of magnetic structures (skyrmions or vortexes). The transition matrix $T$ can be found from the Lippmann–Schwinger integral equation, [15] $\hat{T} = \hat{V} + \hat{V}\hat{G}_0\hat{T}$, where $\hat{G}_0$ is a retarded free electron Green's function, $G_0^{ss'}(\mathbf{k} - \mathbf{k}') = [\varepsilon - \hbar^2k^2/2m \pm J]^{-1}\delta_{ss'}\delta(\mathbf{k} - \mathbf{k}')$. In the Lippmann–Schwinger equation, $\hat{V}$ is a $2 \times 2$ matrix determined by the localized magnetic moment texture:[16]

$$\hat{V}(\mathbf{r}) = -JS_0 \begin{pmatrix} n_z - 1 & n_x - in_y \\ n_x + in_y & -n_z + 1 \end{pmatrix}. \tag{5}$$

Here $n_x^2 + n_y^2 + n_z^2 = 1$. For the calculations, we select the following analytic forms for the skyrmions and for vortexes: $n_z(r) = \cos[\pi(1 - exp(-r^2/a^2))]$ (the topological charge equals ± 1), $n_z(r) = \cos[\pi(exp(-r^2/a^2) - exp(-(c_1 r)^2/a^2))c_2]$ (the topological charge equals 0). The coefficients $c_1$ and $c_2$ allow us to change the minimum location and normalize the spin distribution function. For the calculations we choose $c_1 = 3.2$, that places minimum approximately at $r = 0.5a$, and $c_2 \simeq 1.4255$. For both skyrmion and vortex, the $x$- and $y$-components of the spin textures are determined as $n_x = \cos(\varphi)\sqrt{1 - n_z^2}$ and $n_y = -\sin(\varphi)\sqrt{1 - n_z^2}$, respectively. Here $\varphi$ is a polar angle.

The $T$-matrix has been determined numerically in all orders of $V$ by applying the Fourier transform with respect to the angle between incident and scattered waves. The unknown Fourier coefficients have been found from the Lippmann–Schwinger integral equation. As soon as the transition matrix is calculated, and, therefore the transition probabilities (see Eq. (4)), we substitute $W_{\mathbf{pp}'}^{ss'}$ into the collision integral matrix for $x$-, $y$-components of $\chi^{\uparrow,\downarrow}(\varepsilon)$, which determines the nonequilibrium part of the total distribution function, which has been calculated using the original codes. As soon as the nonequilibrium part of the distribution function is numerically detremined, the electric current can be easily found and presented in the following way (the derivations are given in Supplementary Materials): [11]

$$\begin{aligned} j_x^s &= a_{11}^s eE_x + a_{12}^s eE_y + b_{11}^s \nabla_x(k_B T) + b_{12}^s \nabla_y(k_B T), \\ j_y^s &= a_{21}^s eE_x + a_{22}^s eE_y + b_{21}^s \nabla_x\left(k_B T\right) + b_{22}^s \nabla_y\left(k_B T\right), \end{aligned} \tag{6}$$

where coefficients $a$ and $b$ have been found from the solution of the Boltzmann equation in the low temperature limit. Then, we express SDS, $\alpha$, and SDN, $Q$, coefficients defined by Eq. (3) in terms of $a$ and $b$ coefficients from Eq. (6) under the following conditions: $j_x = j_x^{\uparrow} + j_x^{\downarrow} = j_y = j_y^{\uparrow} + j_y^{\downarrow} = \nabla_y\left(k_B T\right) = 0$. Solving the system of equations we obtain the following expressions for $\alpha$ and $Q$:

$$\alpha = \frac{a_{12}b_{21} - a_{22}b_{11}}{a_{11}a_{22} - a_{12}a_{21}}; \quad Q = \frac{a_{11}b_{21} - a_{21}b_{11}}{a_{12}a_{21} - a_{22}a_{11}}, \tag{7}$$

where $a_{ij} = a_{ij}^{\uparrow} + a_{ij}^{\downarrow}$ and $b_{ij} = b_{ij}^{\uparrow} + b_{ij}^{\downarrow}$. $\alpha$ and $Q$ are presented in Figs. 1–5 for different skyrmion/vortex sizes $\varkappa a$ and $\Gamma$. Here $\varkappa$ and $\Gamma$ are defined as $\varkappa = \sqrt{2mJ}/\hbar$, and $\Gamma = \varepsilon_F/J$. It is known that for a 2D free electron gas Fermi energy, $\varepsilon_F$, is proportional to a carrier concentration, i. e. $\Gamma$ can be regulated using gate voltage or doping concentration. In addition, we have derived that $\alpha$ and $Q$ are proportional to $T$ at low temperatures ($k_B T/J \ll 1$, $k_B T/(\varepsilon_F \pm J) \ll 1$). The proof of this with the detailed derivations is given inSupplementary Materials. In Fig. 1 $\varkappa a = 0.05$, the size of the magnetic structure is very small. In this case, the spin-dependent Seebeck coefficient is of the same order as for other sizes, but the spin-dependent Nernst coefficient is extremely low: it is five orders of magnitude smaller than $\alpha$. The Seebeck coefficient dependencies for different topological charges (i. e., for the skyrmion and vortex) are graphically indistinguishable, and the Nernst coefficients

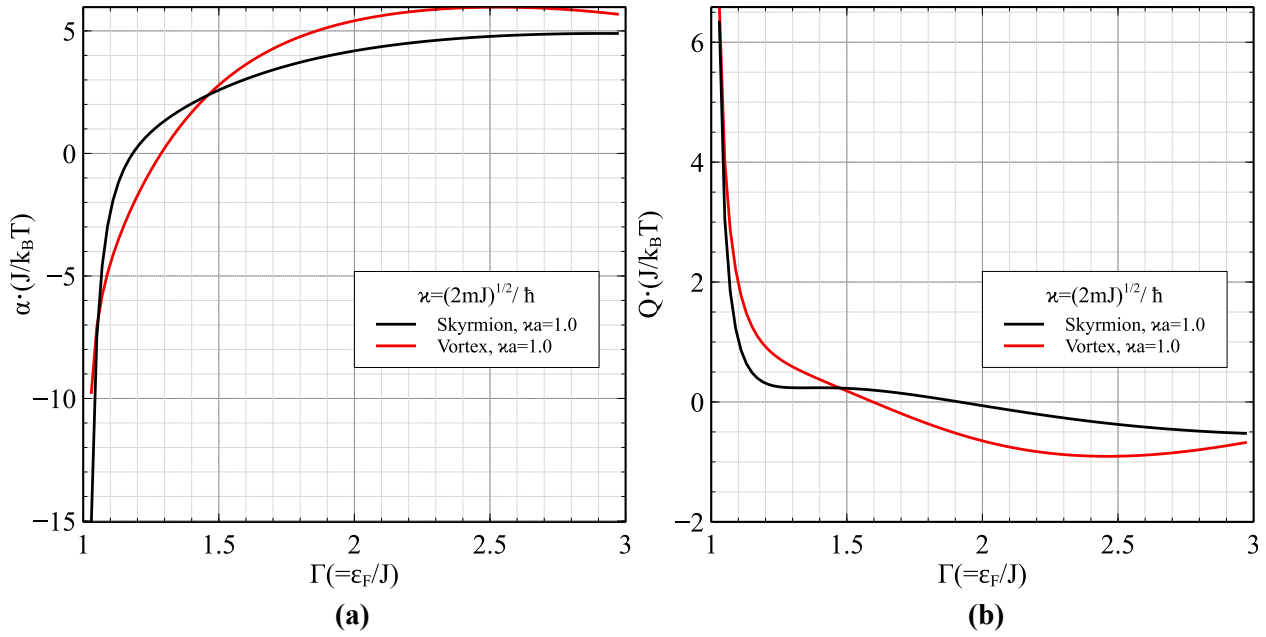


**Fig. 2.** (a) Seebeck coefficient and (b) Nernst coefficient for skyrmion/vortex sizes $\varkappa a = 1.0$.

are also very close. The indistinguishability of the the Seebeck and Nernst coefficients for the skyrmions and vortexes can be explained by the small size with respect to the electron de Broglie wavelength, which is much larger than the magnetic texture size. In this case the scattering is insensitive to the internal spin structure of the texture. Both coefficients decrease with $\Gamma$. The Nernst coefficient exhibits the peak at $\Gamma \approx 1.1$ for both skyrmion and vortex.

For $\varkappa a = 1.0$ the thermoelectric coefficients are presented in Fig. 2. The Seebeck and Nernst coefficients are of the same order now. We note that the both coefficients change their signs, the Seebeck coefficient at $\Gamma \approx 1.2$ for the skyrmion and $\Gamma \approx 1.3$ for the vortex and Nernst coefficient at $\Gamma \approx 1.6$ for the skyrmion and $\Gamma \approx 1.9$ for the vortex. In addition, all coefficients demonstrate the abrupt change at $\Gamma \sim 1$, the Seebeck coefficients are increasing while the Nernst coefficients are decreasing with $\Gamma$.

The thermoelectric coefficients with the relatively large values of the skyrmion size, $\varkappa a = 5.0$ are presented in Fig. 3. The spin-dependent Seebeck coefficient (Fig. 3a) for the vortex has the sharp peak at $\Gamma = 1.15$. It abruptly changes to the minimum at $\Gamma = 1.25$. The skyrmion spin -dependent Seebeck coefficient has the broad minimum at $\Gamma = 1.15$ and then reaches the highest point at $\Gamma \approx 2.5$. The difference between the minimum and maximum values is approximately as much as twice greater the vortex. The picture for the Nernst coefficient (Fig. 3b) is substantially different. For the vortex it is much sharper at $\Gamma = 1.15$, and it has the larger value than for the skyrmion. The skyrmion demonstrates the broad peak at $\Gamma = 1.15$ and the broad minimum at $\Gamma = 1.9$. We note that the thermoelectric coefficients for both magnetic textures change the sign in the range $1 < \Gamma < 3$.

The spin-dependent thermoelectric coefficients for $\varkappa a = 7.0$ are depicted in Fig. 4. In this case, the both vortex Seebeck and Nernst

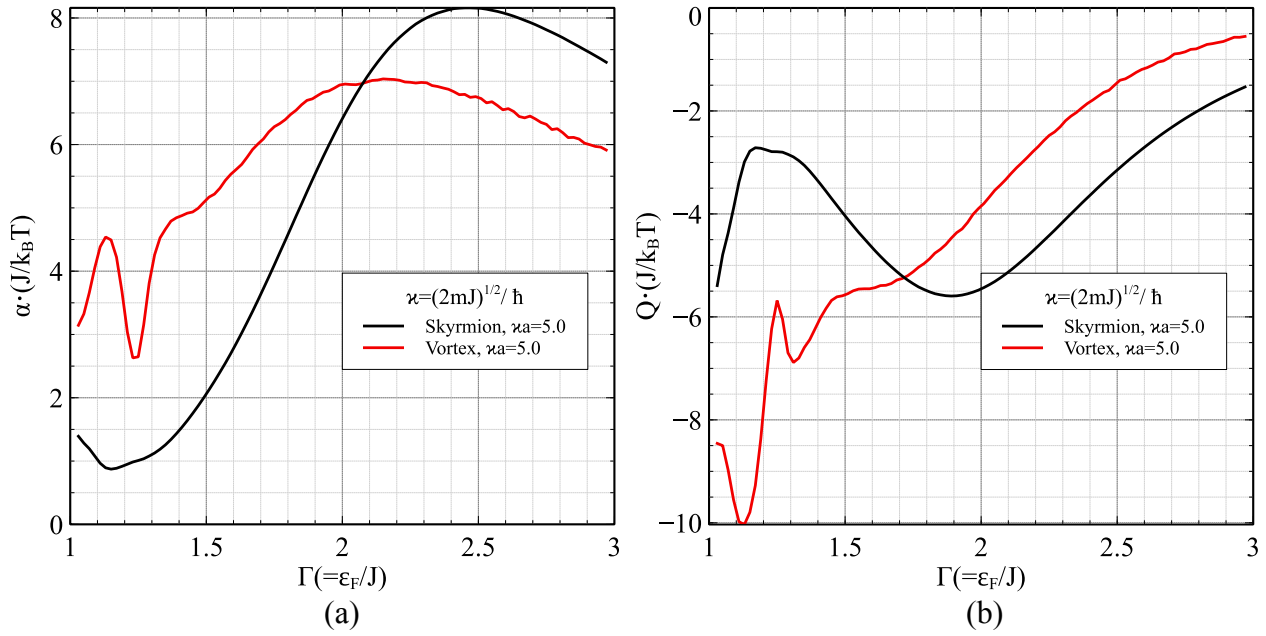


**Fig. 3.** (a) Seebeck coefficient and (b) Nernst coefficient for skyrmion/vortex sizes $\varkappa a = 5.0$.

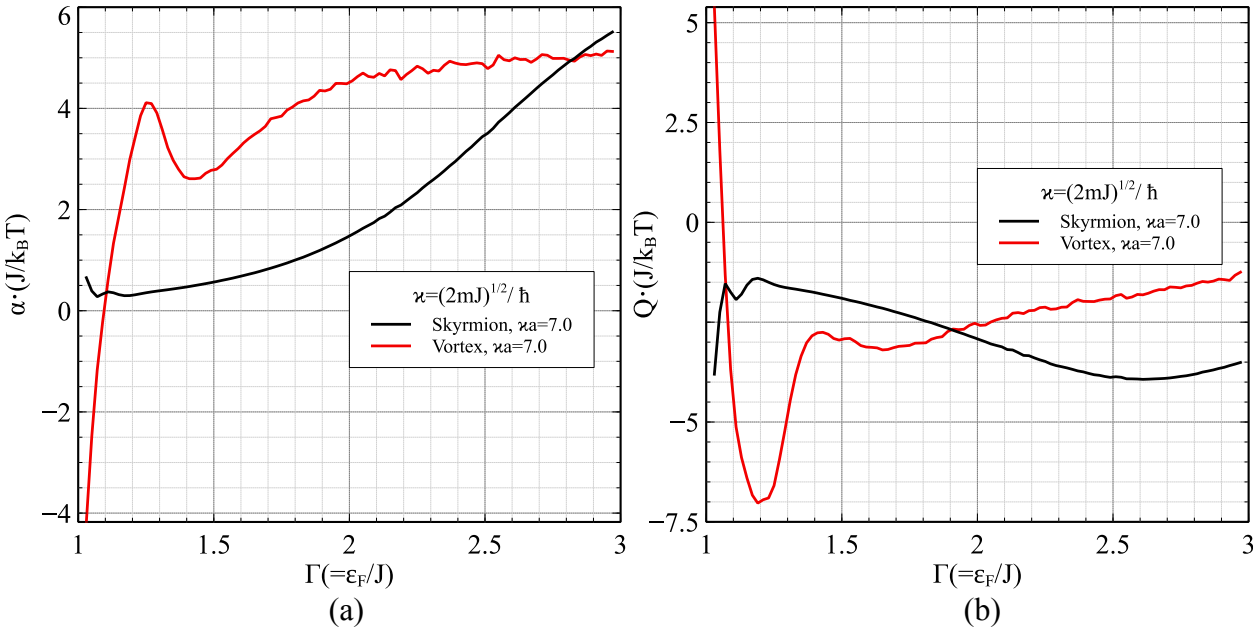


**Fig. 4.** (a) Seebeck coefficient and (b) Nernst coefficient for skyrmion/vortex sizes $\varkappa a = 7.0$.

coefficients demonstrate the dramatic change sign switch at $\Gamma = 1.0$. The Seebeck coefficient has the peak at $\Gamma = 1.25$ and reaches the minimum at $\Gamma = 1.4$. The vortex Nernst coefficient exhibits the sharp minimum at $\Gamma = 1.2$. The skyrmion Seebeck coefficient constantly increases in the whole $\Gamma$ region. The Nernst coefficient for the skyrmion demonstrates the slow change withs the maximum at $\Gamma = 1.2$ and the minimum at $\Gamma = 2.6$.

The spin-dependent thermoelectric coefficients for the large magnetic structure size $\varkappa a = 10.0$ are presented in Fig. 5. The Seebeck coefficient for the vortex rapidly rises from $-12.5$ at $\Gamma = 1$ to 1 at $\Gamma = 1.2$ and then maintains the level of 2.5 starting at $\Gamma = 1.5$. The SDS coefficient for the skyrmion constantly increases from 0 to 2 in this region. The SDN coefficient for the vortex also dramatically changes from its very sharp maximum having the value of 6 at $\Gamma = 1.1$ to the minimum with the value of $-2$ at $\Gamma = 1.2$. It also has a local maximum at $\Gamma = 1.35$. The SDN coefficient for the skyrmion behaves in a similar to the case of $\varkappa a = 7.0$. Indeed, it has a very broad maximum of $-0.75$ at $\Gamma \approx 1.25$ and decreases constantly after that, reaches the value of $-2.5$ at the end of the region.

*In conclusion*, we have analytically and numerically studied the topological spin-dependent Seebeck and Nernst effects in the presence of magnetic skyrmions and vortexes of different sizes. The skyrmion size dependence is nontrivial according to our calculations. First, it depends on a spin projection, second it depends on the electron concentration, and third it could increase or decrease depending on a topological charge.

To explain the independence of the thermoelectric coefficients on a topological charge we have to introduce an adiabaticity parameter $\alpha$. In this work the numerical technique allows us to study the whole range of the adiabaticity, i.e., the $\lambda = k_F a/\Gamma = \varkappa a/\sqrt{\Gamma}$ (see Ref. [13]). Thus, for

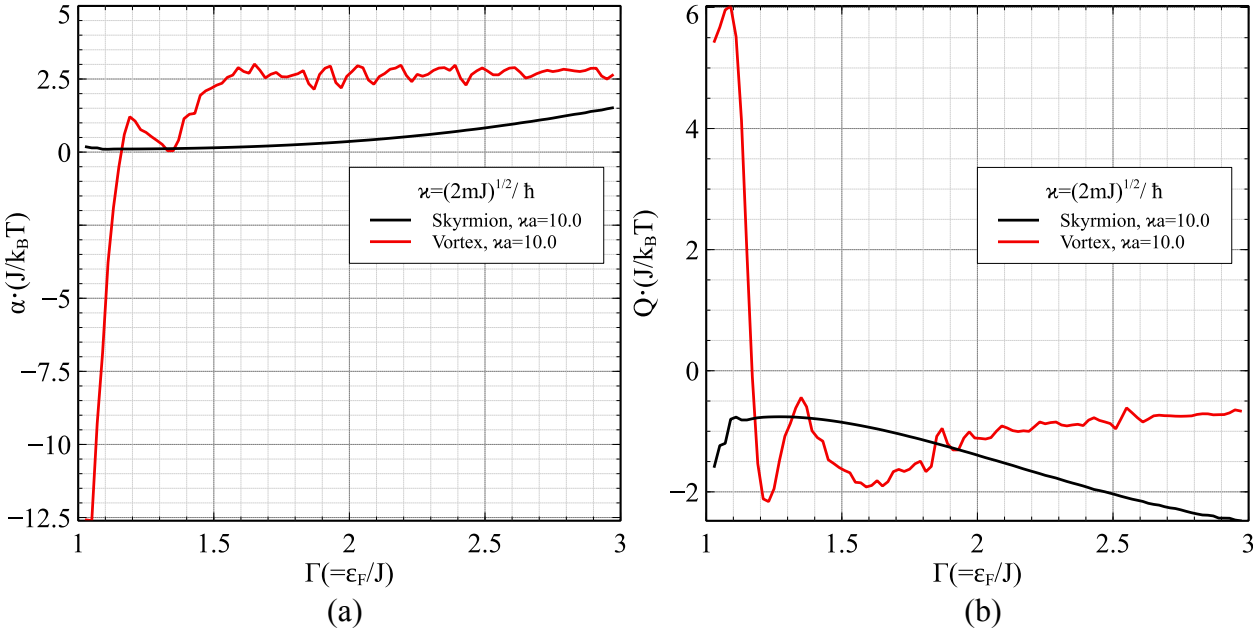


**Fig. 5.** (a) Seebeck coefficient and (b) Nernst coefficient for skyrmion/vortex sizes $\varkappa a = 10.0$.

small sizes ($\varkappa a$) the regime is nonadiabatic. In the adiabatic limit (large $\lambda$), $\varkappa a$ is large and $\Gamma$ is about one. The independence of the SDS and SDN coefficients on topological charge, $Q$, can be explained in terms of adiabaticity. Indeed, in this case $\lambda < 0.05$. Therefore, the scattering spin weakly interacts with the localized magnetic moment. In this case the internal magnetic moment structure is irrelevant. Consequently, we observe indistinguishable Q-dependences for small skyrmion sizes.

The dramatic sign change in both coefficients for the vortex is shown in Figs. 4 and 5 where the sign switching occurs in the narrow region of $\Gamma$s (or electron concentrations). As shown in Fig. 4b, the normalized SDN coefficient changes from + 5 to − 7. The SDS and SDN coefficients are proportional to $T$ at low temperatures. Such a behavior could be useful for a voltage switching in a device where $\varepsilon_F$ can be varied by a gate voltage in the narrow region.

## CRediT authorship contribution statement

**Andrei Zadorozhnyi:** Software, Visualization, Writing - review & editing, Formal analysis, Methodology, Project administration. **Yuri Dahnovsky:** Conceptualization, Investigation, Methodology, Writing - review & editing.

## Declaration of Competing Interest

The authors declare that they have no known competing financial interests or personal relationships that could have appeared to influence the work reported in this paper.

## Acknowledgments

This work was supported by a grant from the U S National Science Foundation (No. DMR-1710512) and the U S Department of Energy (No. 1004389) to the University of Wyoming.

## Appendix A. Supplementary data

Supplementary data associated with this article can be found, in the online version, at https://doi.org/10.1016/j.jmmm.2020.167367.

## References

[1] C. Fang, C. Wan, C. Guo, C. Feng, X. Wang, Y. Xing, M. Zhao, J. Dong, G. Yu, Y. Zhao, X. Han, Observation of large anomalous Nernst effect in 2D layered materials $Fe_3GeTe_2$, Appl. Phys. Lett. 115 (2019) 212402 .
[2] J, Xu, W.A., Phelan, C.-L. Chien, Large anomalous Nernst effect in a Van der Waals ferromagnet $Fe_3GeTe_2$, Nano Lett. 19 (2019) 8250–8254.
[3] C.D.W. Cox, A.J. Caruana, M.D. Cropper, K. Morrison, Anomalous Nernst effect in $Co_2MnSi$ thin films, J. Phys. D: Appl. Phys. 53 (2019) 035005 .
[4] P. Sheng, Y. Sakuraba, Y. Lau, S. Takahashi, S. Mitani, M. Hayashi, The spin Nernst effect in tungsten, Sci. Adv. 3 (2017) e1701503 .
[5] A.S. Melo, A.B. de Oliveira, C. Chesman, R.D. Della Pace, F. Bohn, M.A. Correa, Anomalous Nernst effect in stressed magnetostrictive film grown onto ßexible substrate, Sci. Rep. 9 (2019) 15338.
[6] M. Mizuguchi, S. Nakatsuji, Energy-harvesting materials based on the anomalous Nernst effect, Sci. Technol. Adv. Mater. 20 (2019) 262–275.
[7] R. Ramos, M. Aguirre, A. Anadón, J. Blasco, I. Lucas, P. Algarabel, L. Morellón, E. Saitoh, M. Ibarra, Anomalous Nernst effect of $Fe_3O_4$ single crystal, Phys. Rev. B 90 (2014) 054422 .
[8] K. Uchida, S. Takahashi, K. Harii, J. Ieda, W. Koshibae, K. Ando, S. Maekawa, E. Saitoh, Observation of the spin Neebeck effect, Nature 455 (2008) 778–781.
[9] G.E.W. Bauer, E. Saitoh, B.J. van Wees, Spin caloritronics, Nat. Mater. 11 (2012) 391–399.
[10] Z. Yang, E.A. Codecido, J. Marquez, Y. Zheng, J.P. Heremans, R.C. Myers, Scalable Nernst thermoelectric power using a coiled galfenol wire, AIP Adv. 7 (2017) 095017 .
[11] A. Anselm, Introduction to Semiconductor Theory (Mir, Moscow, 1981).
[12] K.S. Denisov, I.V. Rozhansky, N.S. Averkiev, E. Lahderanta, Electron scattering on a magnetic skyrmion in the nonadiabatic approximation, Phys. Rev. Lett. 117 (2016) 027202 .
[13] K.S. Denisov, I.V. Rozhansky, N.S. Averkiev, E. Lahderanta, General theory of the topological Hall effect in systems with chiral spin textures, Phys. Rev. B 98 (2018) 195439 .
[14] N.A. Sinitsyn, Semiclassical theories of the anomalous Hall effect, J. Phys. Condens. Matter 20 (2007) 023201 .
[15] J.R. Taylor, Scattering Theory: The Quantum Theory on Nonrelativistic Collisions, Wiley, New York, 1972.
[16] N. Nagaosa, Y. Tokura, Topological properties and dynamics of magnetic skyrmions, Nat. Nanotechnol. 8 (2013) 899–911.